Ultrafast Conductivity Dynamics in Colossal Magnetoresistance Manganites

R. D. Averitt,[1,*] A. I. Lobad,[1] C. Kwon,[2] S. A. Trugman,[1] V. K. Thorsmølle,[1] and A. J. Taylor[1]

[1]*Los Alamos National Lab, MS K764, Los Alamos, New Mexico 87545*

[2]*Department of Physics, California State University–Long Beach, Long Beach, California 90840*

Ultrafast picosecond measurements of optically induced changes in the absolute conductivity (0.4–1.0 THz) of $La_{0.7}M_{0.3}MnO_3$ thin films (M = Ca, Sr) from 10 K to $\sim 0.9 T_c$ reveal a two-component relaxation. A fast, ~ 2 ps, conductivity decrease arises from an optically induced modification of the effective phonon temperature. The slower component, related to spin-lattice relaxation, has a lifetime that increases upon approaching T_c from below in accordance with an increasing spin specific heat. We show that, for $T \ll T_c$, $\partial\sigma/\partial T$ is primarily determined by thermally disordered phonons while spin fluctuations dominate near T_c.

The observation of "colossal" negative magnetoresistance (CMR) in the hole-doped manganite perovskites ($R_{1-x}D_xMnO_3$, where, e.g., R = La, Nd and D = Ca, Sr) demonstrates the sensitivity of electronic conduction to the underlying magnetic structure in these materials [1,2]. Experimental and theoretical work has also revealed the importance of the lattice and orbital degrees of freedom in determining the electronic properties of CMR materials above and below T_c [3,4]. Nonetheless, it is still not clear, especially for $T \ll T_c$, what the relative importance of phonons is in comparison to double exchange in determining σ.

Ultrafast optical spectroscopy has provided significant insight into electron dynamics in metals [5–7], and more recently, transition metal oxides [8–10]. Using similar ultrafast techniques, we address the relative contributions of spin fluctuations and phonons in determining the conductivity in the manganites from ~ 10 K to $0.9 T_c$.

Terahertz time-domain spectroscopy is an ultrafast optical technique in which electric field transients are used to measure the complex conductivity of a material. Since this is a coherent technique, a sample can be optically excited and then probed with a terahertz (THz) pulse to measure induced conductivity changes with picosecond (ps) resolution. We use this method, known as time-resolved terahertz spectroscopy (TRTS), to measure ps conductivity transients in $La_{0.7}Ca_{0.3}MnO_3$ (LCMO) and $La_{0.7}Sr_{0.3}MnO_3$ (LSMO) thin films. The dynamics occur on two time scales. A fast, ~ 2 ps, conductivity decrease arises from optically induced modification of the effective phonon temperature. The slower component, related to spin-lattice relaxation, has a lifetime that increases upon approaching T_c from below in accordance with an increasing spin specific heat. Our results demonstrate that, at low temperatures, $\partial\sigma/\partial T$ is primarily determined by thermally disordered phonons while spin fluctuations dominate close to T_c.

The TRTS experiments were performed on LCMO and LSMO epitaxial thin films grown on $LaAlO_3$ substrates using pulsed laser deposition [11]. For very thin films (~ 150 Å), island growth can alter the film properties, but the thicker films used in these experiments (~ 1000 Å) display bulk behavior [12]. Magnetization measurements yield T_c = 250, 360 K for the LCMO and LSMO films, respectively. The experiments utilized a regeneratively amplified Ti:Al_2O_3 system operating at 1 KHz and producing nominally 1.0-mJ, 150-fs pulses at 1.5 eV. The absorbed fluence for LCMO (LSMO) was 170 (110) $\mu J/cm^2$ corresponding to an initially excited carrier density of $\sim 8 \times 10^{19}$ (4×10^{19}) cm^{-3}. The THz pulses were generated and detected using electro-optic techniques. A He cryostat permitted temperature dependent measurements from 4–400 K. Further details of the film growth and TRTS experiments are described elsewhere [11,13].

Figure 1(a) shows the THz electric field transmitted through a LCMO film at various temperatures without optical excitation. The magnitude decreases with decreasing temperature while the phase is relatively constant. This indicates an increase in the real conductivity as the temperature is lowered. Figure 1(b) displays the real conductivity versus frequency for the LCMO film at various temperatures as determined from the data in Fig. 1(a). These conductivity measurements are in the regime $\omega\tau \ll 1$ (ω is the angular frequency and τ is the carrier collision time) as indicated by the flat frequency response. Figures 1(c) and 1(d) show the temperature dependence of σ_r at 0.7 THz for the LCMO and LSMO films, respectively. The lines are fits to the conductivity using the following equation:

$$\sigma(T) = \sigma_o e^{M(T)/M_o}, \qquad (1)$$

where $M(T) \propto (1 - T/T_c)^\beta$ ($\beta \simeq 0.33$) is the magnetization and T_c is the transition temperature. This suggests, in agreement with dc resistivity measurements, that the conductivity is primarily determined by the magnetization below T_c [14]. However, this dependence on the magnetization cannot fully describe the nature of the conductivity
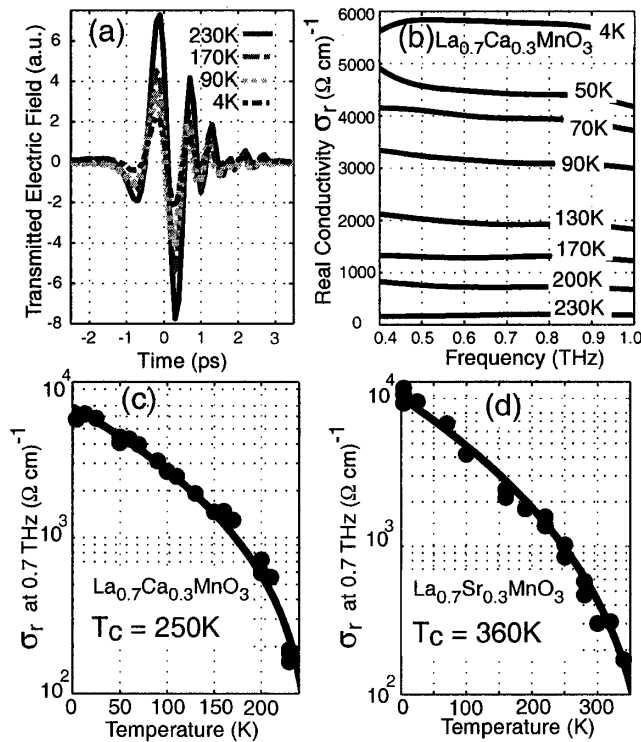
FIG. 1. Temperature dependence of the THz transmission and real conductivity. (a) Transmitted electric field at various temperatures for a 90-nm thick LCMO film. (b) Real conductivity versus frequency for LCMO at various temperatures. (c),(d) The value of the real conductivity at 0.7 THz as a function of temperature for LCMO and LSMO thin films. The lines are fits using Eq. (1).

in the manganites as indicated in more recent experiments [15,16]. As shown below, our dynamic measurements also deviate from Eq. (1).

Figure 2(a) shows the temporal evolution in the normalized peak THz electric field (plotted as $1 - \Delta E$, where ΔE is the induced change in the transmitted electric field) transmitted through a LCMO film following optical excitation at 15, 70, 180, and 230 K. Two components characterize the increase in field transmission. The fast ~2 ps component is resolution limited. However, the data in Fig. 2(a) show this component decreases in magnitude as the temperature is increased. The data in Fig. 2(a) also reveal a slow component that increases in relative magnitude as the temperature is increased. As the temperature is increased the lifetime of the slow component increases.

In Figs. 2(b) and 2(c) the temporal evolution of the optically induced change in absolute conductivity at various temperatures is plotted for the LCMO and LSMO films. In each sample the fast component decreases in absolute magnitude and in relative magnitude to the slow component as the temperature is increased. The lifetime of the slow component increases with temperature for both films. The plateau in the conductivity at longer times corresponds to equilibrium between the electrons, spins, and phonons, albeit at a higher temperature than before the arrival of the

pump. On a ns time scale the film recovers to the initial temperature as the phonons leave the film via thermal transport to the substrate.

To understand the measured dynamics, we consider a model where the spins and lattice are coupled subsystems having well defined temperatures T_s and T_p, respectively:

$$C_p \frac{\partial T_p}{\partial t} = -G_{sl}(T_p - T_s), \qquad (2)$$

$$C_s \frac{\partial T_s}{\partial t} = +G_{sl}(T_p - T_s). \qquad (3)$$

These differential equations describe the energy transfer between the phonons and spins. C_p (C_s) is the lattice (spin) specific heat and G_{sl} is the spin-lattice coupling constant. The initial optical excitation creates a distribution of excited electrons with the same spin orientation as in the ground state, since the initial and final states are coupled via dipole-allowed matrix elements which forbid spin flip transitions. Furthermore, most mechanisms which flip spins conserve total spin. Thus, the initial 2-ps decrease in the conductivity is not related to an ultrafast demagnetization, but rather to a change in the phonon temperature as the excited electrons relax through electron-phonon coupling. Equations (2) and (3) describe the dynamics subsequent to this electron-phonon equilibration. On a longer time scale, spin reorientation occurs due to the combined effects of spin-orbit coupling and momentum scattering (i.e., a scattering process which breaks translational invariance is required in addition to spin-orbit coupling [17]). We attribute the longer time-scale conductivity dynamics to such a process and use Eqs. (2) and (3) to describe this spin-lattice relaxation.

Figures 3(a) and 3(b) show the measured lifetimes of the slow component as a function of temperature for LCMO and LSMO. The solid lines are calculations from numerically solving Eqs. (2) and (3) using fits to the specific heat data of [18] (LCMO) and [19] (LSMO). The spin-lattice lifetime can be approximated as $\tau_{sl} = C_s/G_{sl}$, where G_{sl} is the spin-lattice coupling constant. For these calculations, G_{sl} was assumed independent of temperature. The agreement between experiment and theory in Fig. 3 justifies this assumption yielding $G_{sl} = 2.5 \times 10^{15}$ (5×10^{15}) W/(m^3 K) for LCMO (LSMO).

The results of this two-temperature model can be extended to understand the induced change in conductivity ($\Delta\sigma$) as follows:

$$\Delta\sigma(t, T_p, T_s) = \frac{\partial \sigma}{\partial T_p} \Delta T_p(t) + \frac{\partial \sigma}{\partial T_s} \Delta T_s(t). \qquad (4)$$

This equation shows that the temporal evolution of $\Delta\sigma$ depends on changes in the phonon $\Delta T_p(t)$ and spin $\Delta T_s(t)$ temperatures. It is important to have a measure of the
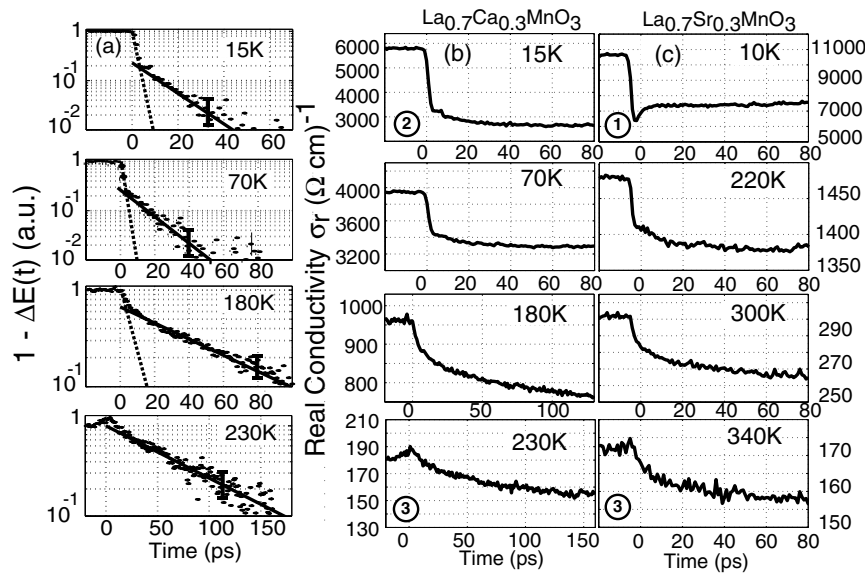
FIG. 2.   (a) One minus the normalized induced change in electric field ΔE versus time for LCMO film at various temperatures (dots). Two slopes are distinguishable—a shorter <2 ps lifetime (dashed line) and a longer lifetime (solid line). (b),(c) Real conductivity versus time at various temperatures. The circled numbers in (b) and (c) correspond to the description in the text using Fig. 4(b). The uncertainty in the data is approximately given by the line thickness. There is also an absolute uncertainty of $\pm 5\%$ due to the uncertainty in the film thickness.

relative importance of phonons and spins in determining σ. Such a measure is given by the quantity

$$\alpha \equiv \frac{\partial \sigma}{\partial T_s} \Big/ \frac{\partial \sigma}{\partial T_p}. \qquad (5)$$

It can be shown that α is given by the ratio of the measured slow component amplitude divided by the fast component amplitude in the limit $C_s \ll C_p$. A plot of α is shown in Fig. 4(a) for LCMO and LSMO as determined from the experimental data in Figs. 2(b) and 2(c). For temperatures less than $\sim 0.5T_c$ ($0.7T_c$) for LCMO (LSMO), α is smaller than 1 indicating that phonons are the primary factor limiting hole transport in the e_g derived conduction band. In contrast, above these temperatures α is larger than 1 and continues to increase with temperature indicating that spin fluctuations predominantly determine σ. For LSMO, $\alpha < 1$ occurs at ~ 0.7, whereas for LCMO this occurs at ~ 0.5. This is consistent with other measurements which indicate that polaronic behavior persists to lower temperatures in LCMO than in LSMO.

The measured α places constraints on the dominant scattering mechanism. If holes are scattered primarily by thermally disordered ions, α would be small, as is observed at low temperatures. If they are scattered primarily by the simple double-exchange mechanism, α would be large, as is observed nearer to T_c. A more subtle case is a polaron/double-exchange scenario in which small polarons form only after the average hopping $\langle t \rangle$ is reduced due to local spin misalignment. Although phonons are involved in this scenario, they are phonons that coherently form a polaron (not thermally disordered phonons), and $\partial \sigma / \partial T_s$ dominates $\partial \sigma / \partial T_p$, resulting in a large α.

It is possible to use the experimental data to extrapolate the conductivity in the T_s-T_p plane by expanding $\ln[\sigma(T_s, T_p)]$ in a power series and performing a least-squares fit using the data in Figs. 4(a) and 1(c). This has been accomplished for LCMO by expanding $\ln(\sigma)$ to third order in T_s and T_p. The results are shown in Fig. 4(b) as contours of constant $\ln(\sigma)$ in the T_s-T_p plane. Conventional measurement techniques (e.g., σ vs T or H) do not deviate from equilibrium as indicated by the white diagonal line in Fig. 4(a). However, TRTS experiments, while starting from a point on the equilibrium line, allow for access to the portion of the T_p-T_s plane below the diagonal equilibrium line since the excited electrons couple preferentially to the phonons during the initial 2 ps. This optically induced change in the phonon temperature is shown by the solid black arrow in Fig. 4(b). The magnitude of this change is given by ξ / C_p, where ξ is the deposited laser energy density. The system then returns to the equilibrium line as shown by the dashed arrows with the slope given by C_p / C_s. Depending on the initial temperature, ξ, and $C_{p,s}$, the observed conductivity decrease can depend predominantly on T_p, T_s, or both.

Figure 4(b) can be used to understand the dynamics shown in Figs. 2(b) and 2(c). The dynamics labeled by a 1 in Fig. 4(b) show a decrease in σ as the lattice temperature increases followed by a slight recovery in the conductivity upon approaching the equilibrium line. In this case the change in σ depends primarily on the phonon temperature. In Fig. 4(b) this is evident in that the contours of constant conductivity are nearly perpendicular to the phonon temperature axis. This is analogous to the data in the first panel of Fig. 2(c), albeit for LSMO. Our model indicates
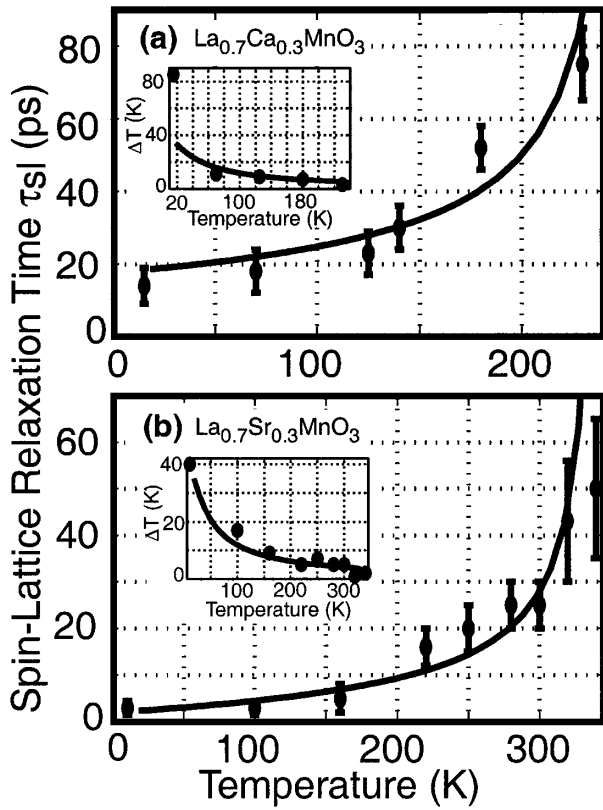
FIG. 3. (a),(b) Temperature dependence of the lifetime τ_{sl} of the slow component due to spin-lattice relaxation for LCMO and LSMO, respectively. The solid lines are fits as described in the text. The inset shows the induced temperature change as determined from the conductivity measurements (dots) and the calculations (solid line).
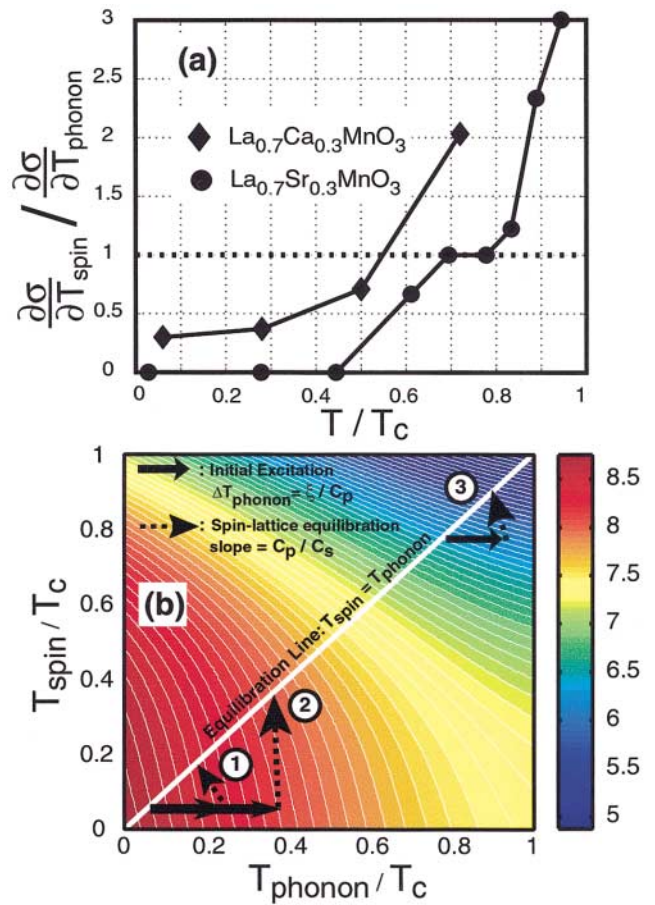

FIG. 4 (color). (a) $\partial\sigma/\partial T_s$ divided by $\partial\sigma/\partial T_p$ versus the initial temperature. The dots (lines to guide the eye) are experimental data. (b) Contours of constant conductivity are plotted in the T_p-T_s plane [the color bar is $\ln(\sigma)$]. The curved white lines highlight the contours of constant conductivity. The arrows labeled 1 to 3 are discussed in the text.

that a slight cooling of the phonon distribution as it transfers heat to the spins accounts for the observed conductivity recovery (i.e., $\partial\sigma/\partial T$ remains negative as expected for the metallic behavior observed at these temperatures). Arrow 2 in Fig. 4(b) again corresponds to a decrease in σ during the initial electron-phonon equilibration, followed by a further decrease in the conductivity as the spin temperature equilibrates with the lattice temperature. This two-component behavior is observed in LCMO at low temperatures [see Fig. 2(b) panel 1] and indeed throughout most of the temperature range for LCMO and LSMO up to higher initial temperatures where, as arrow 3 in Fig. 4(b) shows, the initial change in phonon temperature does not result in a large change in σ: the decrease is due mostly to spin fluctuations. This is evident in that the contours of constant conductivity are now nearly perpendicular to the spin temperature axis. This is observed at higher initial temperatures in both LCMO and LSMO [see the bottom panels of Figs. 2(b) and 2(c)].

In conclusion, we have measured the ultrafast conductivity dynamics in LCMO and LSMO thin films showing that $\partial\sigma/\partial T$ is determined primarily by thermally disordered phonons at low temperatures and by spin fluctuations at higher temperatures.

[1] J. Volger, Physica (Utrecht) **20**, 49 (1954).
[2] S. Jin *et al.,* Science **264**, 413 (1994).
[3] A. J. Millis, Nature (London) **392**, 147 (1998).
[4] *Colossal Magnetoresistive Oxides,* edited by Y. Tokura (Gordon and Breach, Amsterdam, 2000).
[5] G. L. Eesley, Phys. Rev. Lett. **51**, 2140 (1983).
[6] E. Beaurepaire *et al.,* Phys. Rev. Lett. **76**, 4250 (1996).
[7] B. Koopmans *et al.,* Phys. Rev. Lett. **85**, 844 (2000).
[8] J. Demsar *et al.,* Phys. Rev. Lett. **82**, 4918 (1999).
[9] J. S. Dodge *et al.,* Phys. Rev. Lett. **83**, 4650 (1999).
[10] T. Kise *et al.,* Phys. Rev. Lett. **85**, 1986 (2000).
[11] C. Kwon *et al.,* Appl. Phys. Lett. **72**, 486 (1998).
[12] A. Biswas *et al.,* Phys. Rev. B **61**, 9665 (2000).
[13] R. D. Averitt *et al.,* J. Opt. Soc. Am. B **17**, 327 (2000).
[14] M. F. Hundley *et al.,* Appl. Phys. Lett. **67**, 860 (1995).
[15] A. V. Boris *et al.,* Phys. Rev. B **59**, R697 (1999).
[16] G. M. Zhao *et al.,* Phys. Rev. Lett. **84**, 6086 (2000).
[17] Y. Yafet, in *Solid State Physics,* edited by F. Seitz and D. Turnbull (Academic Press, New York, 1963), Vol. 14.
[18] A. P. Ramirez *et al.,* Phys. Rev. Lett. **76**, 3188 (1996).
[19] M. N. Khlopkin *et al.,* Phys. Solid State **42**, 114 (2000).